Single-Frequency 1 μm Laser for Field Applications

Floyd E. Hovis, Charles Culpepper, Tom Schum and Greg Witt
Fibertek, Inc.
510 Herndon Parkway
Herndon, VA 20170

Abstract- **We have just completed the final phase of an Advanced Technology Initiative Program (ATIP) funded effort to develop the 1 μm pump source needed for ozone DIAL and other lidar systems. The output of this program was a brassboard version of a robust, single-frequency oscillator/amplifier that achieved 500 mJ/pulse at 20 Hz with an M^2 of 3 or 300 mJ/pulse at 50 Hz with an M^2 of 1.5.**

I. INTRODUCTION

A critical component of a space-based ozone differential absorption lidar (DIAL) as well as a number of other space-based lidar systems is a space-qualified 1μm pump source that provides single frequency, high energy, and high beam quality pulses. These pump requirements minimize the risk of damage in the system amplifiers as well as any nonlinear converters. They also maximize the efficiency of the nonlinear converters. Although 1μm laboratory lasers can achieve the desired output, the technologies on which these lasers are based are not compatible with the requirement to operate in space. Common shortcomings include the inability to survive the vibrational environment of a launch, sensitivity to thermal variations, and liquid-based cooling for heat removal. The overall objective of our ESTO funded research was the development of 1 μm laser technology that is space-qualifiable and can meet the following design and output characteristics.

1) Scalable to >1 J single frequency pulses.
2) Electrical to optical efficiencies of 10%.
3) Reduced package size and weight.
4) Diode-pumping with conductive cooling of both the diodes and laser gain medium.

In addition to the originally planned ozone DIAL applications for the 1 μm laser developed in this program, a number of other applications were identified during the execution of the project. These additional applications include:

1) Single frequency pump source to generate the UV output required for direct detection wind lidar systems [1,2]
2) Single frequency pump source for use in high spectral resolution lidar (HSRL) systems [2,3].
3) General purpose 1 μm pump source for use in systems that require high pulse energies to generate other wavelengths through nonlinear conversion processes.

Our approach is based on an oscillator/amplifier design. The design incorporates diode-pumped, conductively cooled Nd:YAG slabs as the gain media. The oscillator is a telescopic ring resonator design that can be easily reconfigured for a variety of operational scenarios. An unstable version of the oscillator achieved 125 mJ/pulse with >10% electrical to optical efficiency and an M^2 of 2.5. When operated in a stable TEM_{00} mode, the ring laser demonstrated >30 mJ/pulse at 100 Hz with an M^2 of 1.3. Both configurations of the oscillator were used to extract dual conductively cooled slab amplifiers. Using the 125 mJ output of the unstable ring, we achieved 500 mJ/pulse of amplified output with an electrical to optical efficiency of > 10% and an M^2 of 3. Using the 30 mJ TEM_{00} output of the stable ring we achieved 300 mJ/pulse of amplified output at 50 Hz with an M^2 of 1.5. This report describes design details of the laser system that we developed.

II. RING OSCILLATOR DESIGN AND CHARACTERIZATION

A. Oscillator head design

The first step in the system development was to design, build, and characterize a conductively-cooled, zigzag slab pump head for the oscillator. We chose to use one-sided pumped and cooled Nd:YAG slab technology that has been well developed by a number of investigators [4, 5]. However, transient thermal and phase distortion effects have not been well characterized for the case of two closely spaced (300-400μs) pump and extracting pulses that will be needed for ozone DIAL measurements. One possible source of transient distortion is the partially extracted gain profile from the first pulse that will not have fully decayed before the second pulse. The zigzag slab compensates for the gain and thermal non-uniformities in the plane of the zigzag, but will not compensate for those in the orthogonal axis. As a part of the head design we also measured these transient effects

Our approach to the oscillator head design for our Phase I work was to develop a design that demonstrated the key features needed for a flight system and that could be easily modified for an actual flight build. To this end we developed a design that used a bridge structure to mount and conductively cool the zigzag slab to a pedestal on which the pump diodes were mounted. For this laboratory study the pedestal was conductively coupled to a liquid-cooled plate for heat removal, but the transition to a radiatively cooled interface plate would be straightforward. The slab design was a 6 mm x 6 mm x

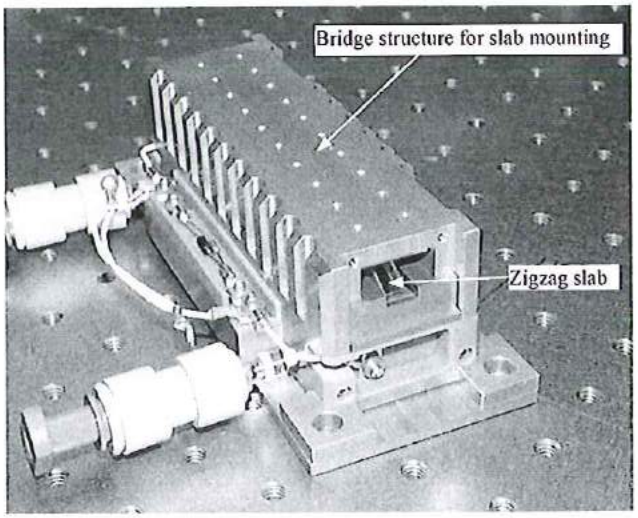

Fig. 1. Conductively cooled laser head.

120 mm zigzag slab (12 bounce) with Brewster angle tips. As will be seen subsequently, the oscillator design provides linear polarization through the slab head, allowing the use of Brewster angle tips and eliminating the need for coating of the entrance and exit faces. Fig. 1 shows the fully assembled pump head.

B. Diode-pumped head characterization

The first measurements we performed on the laser head were fluorescence and gain measurements. A cw Nd:YAG laser aligned through the center of the slab was used to perform a series of single pass gain measurements. A Cohu Model 4812-7000 CCD camera and Spiricon LBA-300PC-CD beam imaging system were used to record the fluorescence profiles in the slab. Both the center gain and total fluorescence were measured as a function of pump pulse width and coolant temperature with the diode bars in the arrays operated at peak powers of 50 W and 60 W. The results of these measurements are summarized below.

1) The maximum single pass gain occurred at a coolant temperature of around 40-45°C. With 200 μs pump pulses, the maximum gain was 12 for 50 W peak power per bar and 19 for 60 W peak power per bar.
2) Both the peak and total fluorescence have the same temperature dependence as the single-pass gain
3) The single pass gain measurements showed a monotonic increase in gain as a function of pump time. This demonstrates that there are no significant parasitic oscillations in the slab.
4) The results showed we could achieve the single-pass gain of ~10-20 required for operation of the unstable ring resonator.

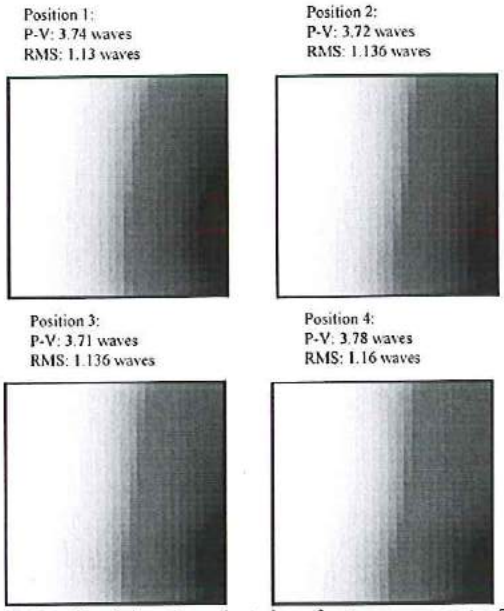

Fig. 2. Results of time dependent phase front measurements. The horizontal axis is in the zigzag plane.

The final set of measurements we performed was a characterization of the phase front distortion induced by the slab gain medium. In particular, we examined whether there was any variation in the phase front distortion from the first to second pulse of the pulse pairs when the pulse pairs occur at a 10 Hz repetition rate. We used a gateable Shack-Hartman interferometer (the CLAS-2D system built by WaveFront Sciences) to measure the distortion of a helium/neon probe beam at four points in time: 1) at the beginning of the first 200 μs pump pulse; 2) at the end of the first pulse; 3) at the beginning of the second 200 μs pump pulse; and 4) at the end of the second pulse. The spacing between the leading edges of the two pump pulses was 400 μs.

The resulting phase front data was fit using both Zernike and XY polynomials to extract the key phase front parameters of the probe beam after passing through the slab. A 0.5 X magnification telescope was used to transform the origin of the camera used in the CLAS-2D system to the slab exit face and to allow the full probe beam to fit within the camera CCD. The calculated phase front parameters were essentially the same whether Zernike or XY fits were performed. The largest contributions to the phase front distortion were determined to be simple tip and tilt of the wavefront. In addition, no significant differences in the phase fronts were found at the four temporal positions that were monitored. Fig. 2 provides visual images of the probe beam phase front at each of the temporal positions after the tip and tilt contributions have been removed. It also gives the peak-to-valley (PV) and RMS wavefront distortion for each temporal position. These results clearly show that there

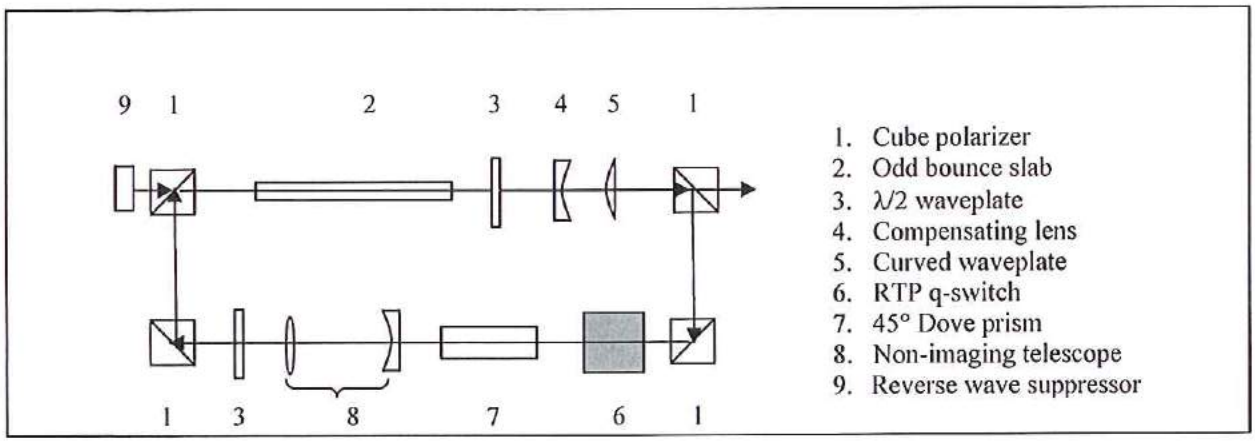

Figure 3. Optical layout for the low expansion Zerodur optical bench

will not be a time-dependent phase front distortion in the output beam of a dual-pulse laser oscillator built around this head.

C. Telescopic ring oscillator design and characterization

For this portion of the design we investigated a telescopic ring oscillator design that could achieve high beam quality, single frequency operation, and the linear polarization preferred for our well-developed slab technology. By combining polarization output coupling with a unidirectional ring, it is possible to establish linear polarization in the section of the ring containing the conductively cooled slab. By including an element with radially varying birefringence in the output coupling section, graded reflectivity output coupling is also accomplished. The combination of operating the ring as an unstable resonator plus graded reflectivity output coupling can achieve a large volume mode for efficient energy extraction, high beam quality, and a supergaussian profile in the output beam. The use of a reverse wave suppressor to establish unidirectional operation eliminates the need for a Faraday isolator, thus reducing both the size an weight of the final system.

During the execution of the program we took advantage of the fact that the ring resonator could be readily reconfigured to meet varying program performance requirements. In order to provide a quantitative basis for future system designs, we characterized the following ring configurations.

1. Telescopic unstable ring oscillator with graded reflectivity output coupling.
2. Stable TEM_{00} ring oscillator with uniform output coupling.

The design and characterization of each of these ring oscillator configurations are described in more detail in the following sections.

1) Design and characterization of a telescopic unstable ring oscillator: The design of the telescopic unstable ring oscillator we developed in this program work is shown schematically in Fig. 3. A picture of the fully populated Zerodur optical bench is shown in Figure 4. It has a number

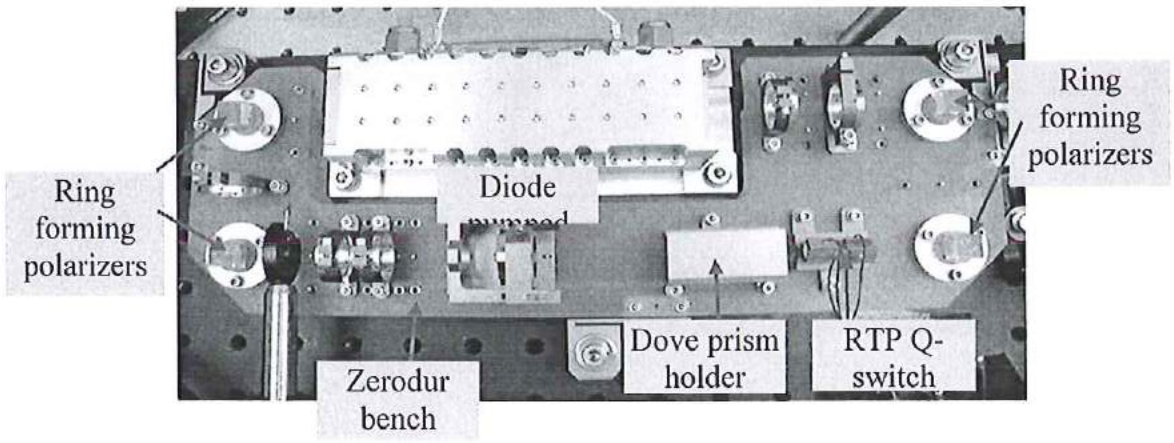

Figure 4. Zerodur optical bench configured as a TEM_{00} ring oscillator

of desirable features, some of which are intrinsic to ring oscillators in general and some of which are unique to this design. These features are summarized below.

1) The traveling wave nature of the ring avoids spatial hole burning in the gain medium and simplifies achieving single frequency operation.
2) 90° polarizers are used to form the ring. This makes the ring more compact, creates a linearly polarized section that allows the use of a Brewster angle slab, and allows the use of a half-wave plate to control the percent output coupling. Any desired value can be achieved by simply rotating the waveplate.
3) The resonator has a low fluence section after the output polarizer (relative to the beam propagation direction) that provides a place to put lower damage threshold components such as Q-switches and etalons.
4) A Dove prism in the low fluence leg of the ring rotates the beam image 90° each round trip. This use of a Dove prism in the ring resonator nearly eliminates the gain and lensing inhomogeneities associated with the one-sided pumping and cooling of the Nd:YAG slab in the oscillator head.
5) The optical bench is made of low expansion Zerodur to improve the boresight and single frequency operation stability. It has a footprint of about 4.5" x 14".
6) Graded reflectivity output coupling is used to achieve a square, supergaussian output beam.
7) The use of a reverse wave suppressor establishes >100/1 unidirectional operation and eliminates the need for a relatively large and heavy Faraday isolator.

The use of graded reflectivity output coupling is an established technique for improving the near field spatial profile of unstable resonators [6]. Since the ring oscillator in this work uses polarization-based output coupling, traditional graded reflectivity output couplers will not work. The approach we have chosen is to use a radially varying thickness waveplate to achieve the desired graded reflectivity output coupling [7]. For this design, a waveplate with a spherical curvature on one surface can achieve the desired output coupling profile. A compensation lens (4 in Fig. 3) is used to correct for the spherical focusing induced by the curved waveplate. The orientation of the curved waveplate is used to control the peak center reflectivity. The 100% output coupling radius is determined by the desired output beam size and the telescope magnification. We assumed a limiting aperture of 5 mm and a telescope magnification of 1.5. Using these assumptions, we modeled the radial dependence of the feed back into the cavity that is achieved as a function of the waveplate curvature. The results showed that a radius of curvature of 40 mm for the curved waveplate would achieve the desired maximum feedback in the 50-60% range. This is the radius for the curved waveplate we used in a resonator to be described below.

Although seeding of the ring to achieve single frequency operation is anticipated for any final fielded design, we used a simplified "self seeded" [8] approach as a lower cost alternative for this study. This approach is based on the observation that for a resonator with good mode selectivity, the first relaxation oscillation is a single transverse and axial mode. By adjusting the hold-off waveplate of the laser to allow a single relaxation to occur and then triggering the Q-switch during this first relaxation oscillation, the relaxation oscillation seeds the build-up of the Q-switched pulse. Since most of the first relaxation oscillations are single frequency, the resulting Q-switched pulses are predominantly single frequency.

Since the original design goal was a 20 Hz laser system, this was the repetition rate that we used for the initial characterization of the telescopic ring oscillator. Measurements on the unstable ring of the electrical power into the diodes vs. q-switched output energy are shown in Figure 5. The final optimized result was an efficiency of 10.5% and an output pulse energy of 135 mJ.

We also measured the beam quality of the non-imaging ring at 20 Hz. Our approach to this measurement is summarized below.

1) Measure a series of beam diameters over several Raleigh ranges that include a beam waist, i.e. point of minimum beam diameter.

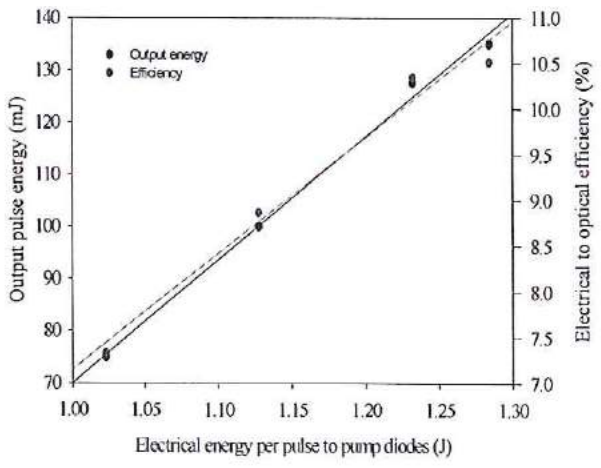

Figure 5. Unstable ring output vs. electrical input at 20 Hz

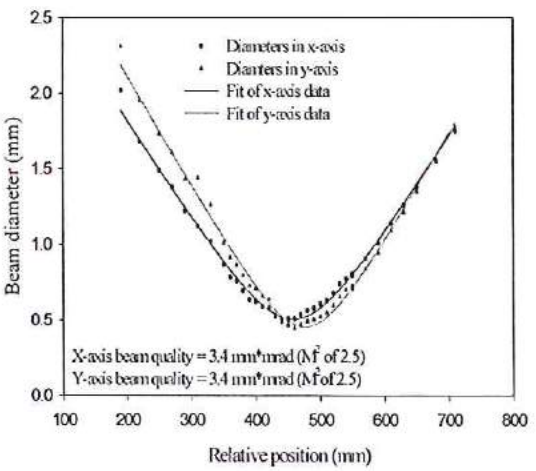

Figure 6. Unstable ring laser beam quality data at 20 Hz

2) Fit the beam diameters as a function of position to the form

$$D(r) = [D_o^2 + \theta_o^2(r - r_o)^2]^{1/2} \quad 1)$$

where D(r) is the beam diameter at the relative position r, D_o is the minimum beam diameter, θ_o is the far field divergence, and r_o is the position of the minimum beam diameter.

3) Calculate the beam quality in mm*mrad by multiplying the D_o by θ_o.
4) For 1064 nm determine the times diffraction limit beam quality (M^2) by dividing the mm*mrad beam quality by the Gaussian beam diffraction limit of 1.35 mm*mrad.
5) Since the beams are astigmatic, we report beam qualities in both the vertical and horizontal axes.

In the experimental set-up for the beam quality measurements we used a Spiricon LBA-300PC system to determine the beam diameters. For the 1064 nm measurements we used Schott RG780 glass as the bandpass filter. Figure 6 shows the data and fits of our 1064 nm beam quality measurements. Notice the improved symmetry due to the use of the Dove prism.

During the execution of this program, an increased interest in the possibility of operating the laser at higher repetition rates with reduced pulsed energies developed. This reduces the risk of optical damage while maintaining or even increasing the average power extractable from the laser. We performed two sets of measurements on the unstable ring laser to quantify its performance at higher repetition rates. The first was a set of 50 Hz measurements of the laser output pulse energies and efficiencies vs. input electrical energy to the pump diodes. The results are shown if Figure 7. Within the experimental uncertainties of the measurements, the optimized pulse energy of 146 mJ and efficiency of 10.4% are equal to the values obtained at 20 Hz.

The second set of measurements determined the variation in output pulse energy as a function of repetition rate. For this measurement the non-imaging ring laser was set up to achieve ~100 mJ/pulse at 50 Hz and then the output pulse energy vs. repetition rate was measured from 10 Hz to 70 Hz with no further adjustments. The results of these measurements are given in Figure 8. They show that the energy is constant to within +/-5% over the entire range of repetition rates.

2) Characterization of the telescopic ring oscillator as a stable TEM_{00} oscillator: Although the non-imaging ring laser easily met the output energy goal of 100 mJ/pulse, achieved an electrical to optical efficiency of >10%, and had stable output energy performance from 10 to 70 Hz, we were not able to get it to meet the beam quality goal of $M^2 < 2$ with the graded reflectivity optics that had been designed for use with the unstable resonator. In order to improve the beam quality we reconfigured the telescopic ring as a stable, TEM_{00} oscillator. Standard ray matrix analysis shows that by appropriately detuning the intra-cavity telescope, a converging TEM_{00} output beam with a relatively large diameter (~3 mm) in the Nd:YAG slab can be achieved. The optical layout we used for the TEM_{00} ring is the same as that shown in Figure 3 with the following changes.

1) The curved waveplate and compensating lens are removed.
2) The intra-cavity telescope spacing is detuned to be slightly longer than the value required to achieve a collimated output beam.
3) A low finesse etalon (surface reflectivities of 30%, 1 cm thick) was added at the input to the slab to improve the frequency stability and reduce the occurrence of modulated pulses when the stable ring was operated in the self-seeded mode described earlier.

Since the beam diameters were relatively small in region of the RTP q-switch, we limited testing of the TEM_{00} ring to pulse energies on the order of 30 mJ. This meant that the diode pump pulse energy was relatively low and that

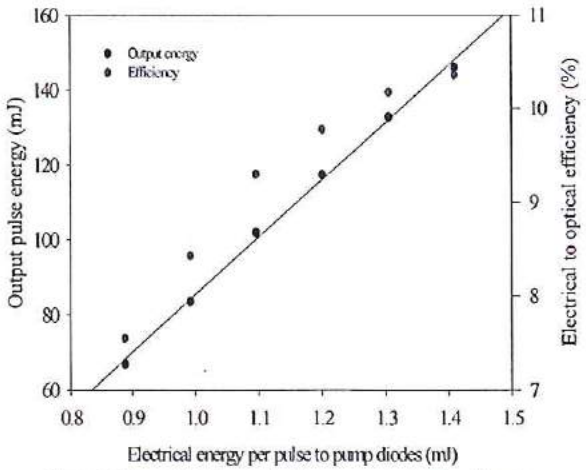

Figure 7. Unstable ring optical output vs. electrical input for 50 Hz operation

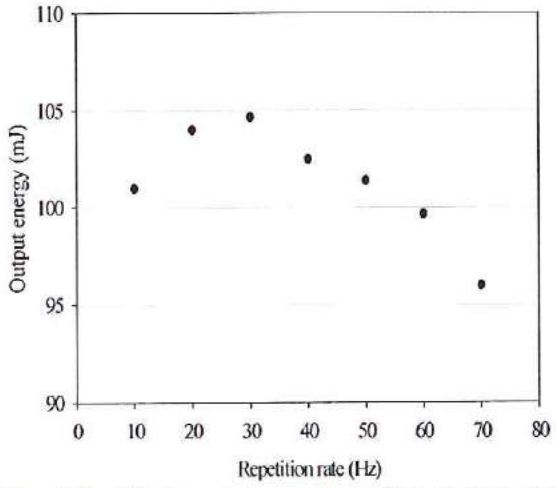

Figure 8. Unstable ring output energy vs. repetition rate for fixed input

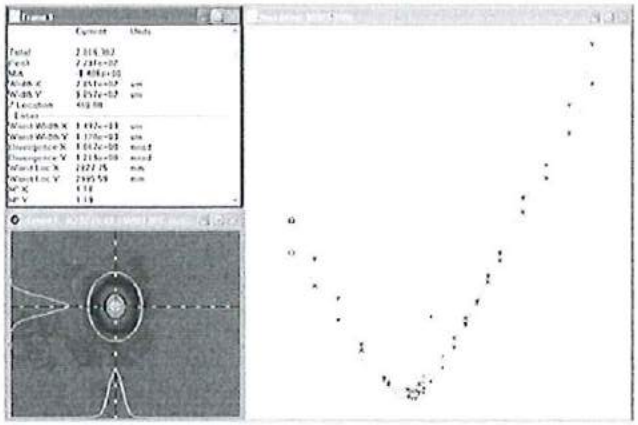

Figure 8. TEM_{00} ring laser 50 Hz beam quality measurement results

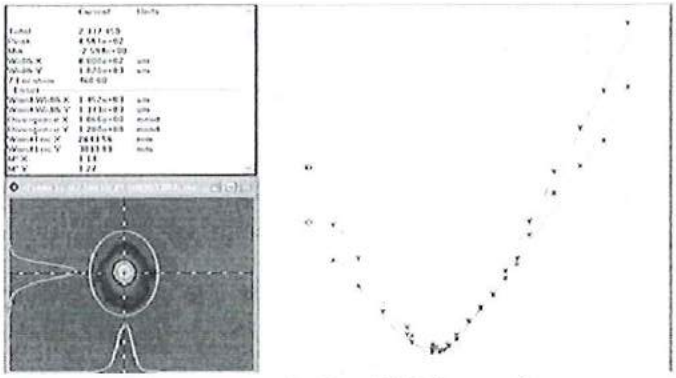

Figure 9. TEM_{00} ring laser 100 Hz beam quality measurement results

operation at higher repetition rates was be possible. To evaluate the performance of the TEM_{00} ring we set it up for 30 mJ/pulse output and measured the beam qualities at 50 Hz and 100 Hz. The approach was the same as that described above. The results of the beam quality measurements were quite good. They are shown in Figures 8 and 9. At 50 Hz the beam qualities in the two axes were essentially the same, both with an M^2 of 1.2. At 100 Hz the beam was slightly elliptical with a horizontal axis M^2 of 1.14 and a vertical axis M^2 of 1.27.

III. AMPLIFIER DESIGN AND CHARACTERIZATION

A. Amplifier design

The design of the final dual slab amplifier is shown in Figure 10. The output beam from the oscillator enters the first slab near normal to the slab face and executes a 15-bounce path. On the fifteen bounce pass, eight of the bounces on one side of the slab are well overlapped with the eight diode arrays that pump the slab in order to maximize absorption of the 808 nm pump light. A mirror pair folds the output of the first slab through a Dove prism set to rotate the beam image by 90° and into the second slab for a 15-bounce path through it. As with the oscillator design, this use of a Dove prism reduces both the gain and lensing asymmetry that is introduced with the use of single-sided pumped and cooled slabs. The output of the second slab is well spatially separated from the original input beam, thus eliminating the need for an optical isolator. We used both the unstable and stable TEM_{00} stable configurations of the telescopic ring oscillator as inputs to the dual slab amplifiers. The results are given below.

B. Amplifier extraction with the unstable ring oscillator

The original goal of this program was to develop a design for relatively low repetition rate (~20 Hz) that was scalable to high pulse energies (~1 J/pulse). To optimize extraction of the amplifiers, it is necessary to use the maximum input possible. As was seen in Section II, the unstable ring configuration with graded reflectivity output coupling gave the highest pulse energies out of the ring oscillator. Thus for determining the highest output pulse energies achievable from the system we used the output from the unstable ring oscillator to extract the amplifiers. The results of measurements of the output energy from the dual slab amplifiers for 115 mJ of input from the ring oscillator are shown in Figure 11. The amplifier electrical to optical efficiency at the highest output energy was 11.3%, exceeding the program goal of 10%.

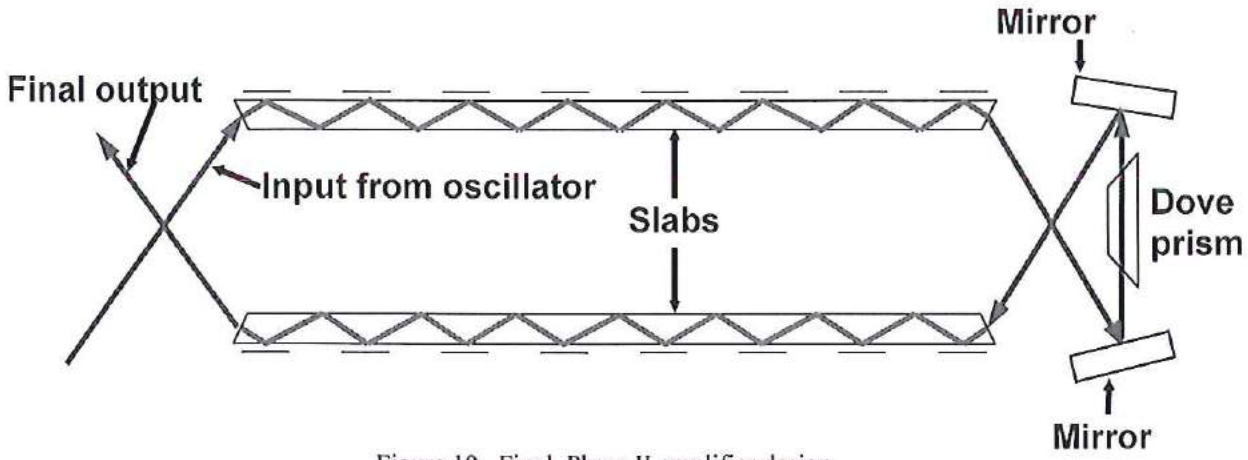

Figure 10. Final Phase II amplifier design

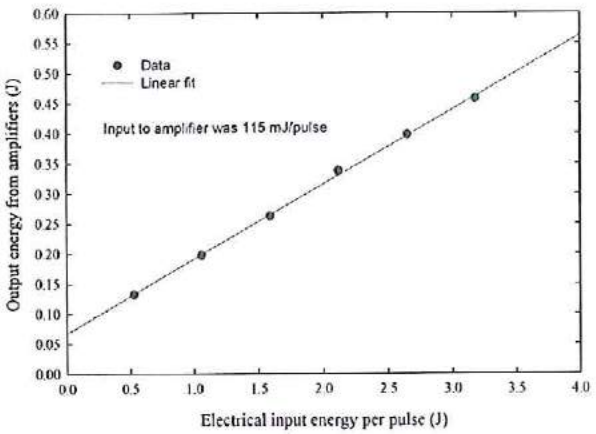

Figure 11. Amplifier optical output vs. electrical input

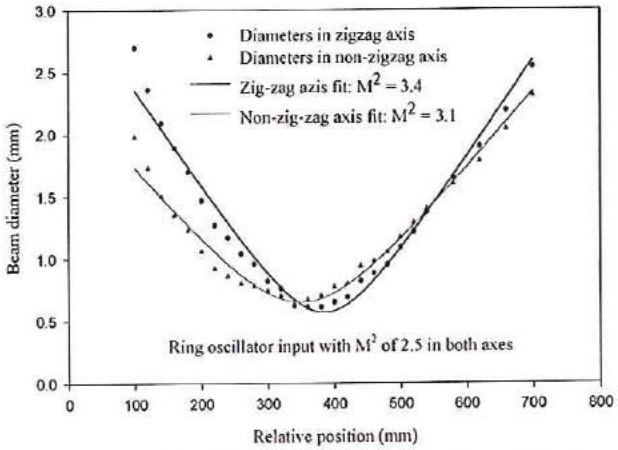

Figure 12. Amplifier output beam quality with unstable ring oscillator input

In addition to the output energy measurements shown in Figure 11, a set of beam quality measurements was made for the highest output pulse energy conditions shown there. The approach and experimental setup is the same as that described in Section II.C. Figure 12 shows the results of the beam quality measurements. The zigzag axis had an M^2 of 3.4 and the non-zigzag axis had an M^2 of 3.1. Since the input beam quality is an M^2 of 2.5 in both axes, this implies that the effective M^2 values of the dual amplifiers are 1.36 in the zigzag axis and 1.24 in the non-zigzag axis. Thus with input beam qualities to the amplifiers of $M^2 <$ 1.4, the desired output beam quality of $M^2 < 2$ could be achieved. These results led us to conclude that we could achieve the desired beam quality at even higher repetition rates if we used the ring resonator in a stable TEM_{00} configuration to extract the amplifiers. The results of such measurements are described in the next section.

C. Amplifier extraction with the TEM_{00} ring oscillator

The amplifier results presented in Section III.B showed that the oscillator/amplifier configuration tested there met the output pulse energy and efficiency goals but the demonstrated M^2 of ~3 fell short of the desired beam quality of $M^2 < 2$. The data did show that the primary driver for the reduced beam quality was the input beam which had an M^2 of 2.5. The effective M^2 of the dual slab amplifier was < 1.4. This implies that if the input beam to the amplifiers had an M^2 of < 1.4 the output of the amplifiers would have an M^2 of < 2.

In Section II.C we showed that the ring laser could be configured as a TEM_{00} stable oscillator with an output of at least 30 mJ/pulse and an $M^2 < 1.4$ when operated at both 50 Hz and 100 Hz. Thus we would expect that if the amplifiers were extracted with the output of the TEM_{00} stable oscillator we would achieve the desired $M^2 < 2$. Using the TEM_{00} stable oscillator at high repetition rates would also allow us to evaluate the possibility of operating the oscillator/amplifier at lower pulse energies but higher repetition rates while maintaining or even increasing the average output power.

We performed measurements to evaluate operation at higher repetition rates as a part of the amplifier characterization. A picture of the final oscillator/amplifier configuration is shown in Figure 13. It has a footprint of about 13" x 19". The system was successfully operated at 50 Hz with an output of 300 mJ/pulse. The input to the amplifiers was 30 mJ of output from the ring configured as a stable TEM_{00} oscillator with an M^2 of ~1.3. Figure 14 shows the results of a series of beam quality measurements that were made on this system configuration. The resulting horizontal M^2 of 1.52 and vertical M^2 of 1.44

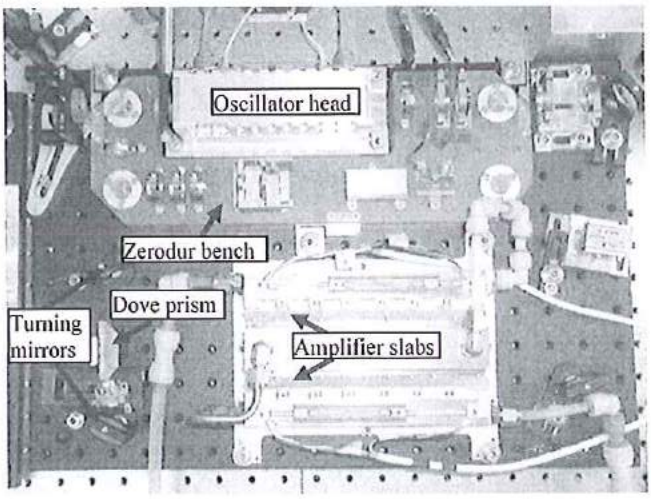

Figure 13. Final oscillator/amplifier configuration

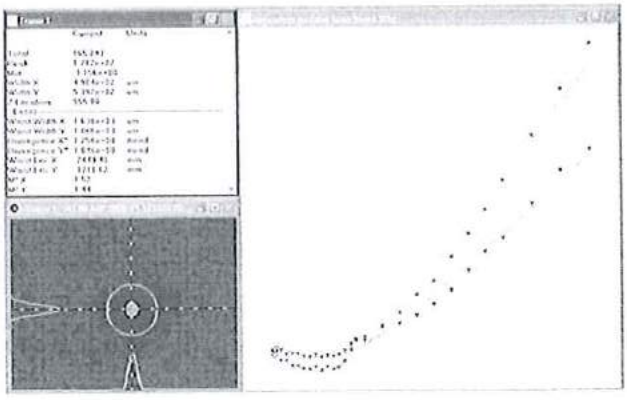

Figure 14. 50 Hz amplifier beam quality with TEM_{00} oscillator input

easily meets the goal of < 2. The results also show that the use of the Dove prism between the amplifier stages to improve the output beam symmetry works even at the higher repetition rates.

ACKNOWLEDGMENTS

We wish to thank the Office of Earth Science and the NASA Langley Research Center for their support of this research and development effort.

REFERENCES

[1] B. M. Gentry, "Tropospheric wind measurements obtained with the Goddard Lidar Observatory for Winds (GLOW): Validation and performance," in *Proc. SPIE*, Anton Kohnle, Ed., vol. 4484, pp. 74-81, 2002.

[2] F. Hovis, M Rhoades, R. Burnham, J. Force, T. Schum, B. Gentry, H. Chen, S. Li, J. Hair, A. Cook, C. Hostetler, "Single frequency lasers for remote sensing", *Proc. SPIE*, R. Scheps and H Hoffman, Eds., vol. 5332, 2004.

[3] J. W. Hair, M. Caldwell, D. A. Krueger, C. Y. She, "High-spectral-resolution lidar with iodine-vapor filters: measurement of atmospheric-state and aerosol profiles," *Appl. Optics*, vol. 40, pp. 5280-5294, 2001.

[4] A. D. Hays, G. Witt, N. Martin, D. Dibiase, R. L. Burnham, "Ultracompact diode-pumped solid state lasers," *Proc. SPIE,* R. Scheps and M. R. Kokta, eds., Vol. 2380, pp. 89-94, 1995.

[5] R. Afzal, "Mars Observer Laser Altimeter: Laser Transmitter", *Appl. Opt.*, vol. 33, pp. 3184-3188 (1994)

[6] A. Siegman, *Lasers,* Mill Valley, Ca, University Science, 1989, Chapt. 23.

[7] J. M Eggleston, G. Giuliani, and R.L. Byer, "Radial intensity filters using radial birefringent elements," *J. Opt. Soc. Am.*, vol. 71, pp. 1264-1272, 1981.

[8] Y. K. Park and R. L. Byer, "Electronic linewidth narrowing method for single axial mode operation of Q-switched Nd:YAG lasers," Optics Comm., vol. 6, pp. 411-416, 1981.